

pubs.acs.org/JPCB Article

# Behavior of Water Near Multimodal Chromatography Ligands and Its Consequences for Modulating Protein—Ligand Interactions

Camille L. Bilodeau,\* Edmond Y. Lau, David J. Roush, Mark A. Snyder, and Steven M. Cramer



Cite This: J. Phys. Chem. B 2021, 125, 6112–6120



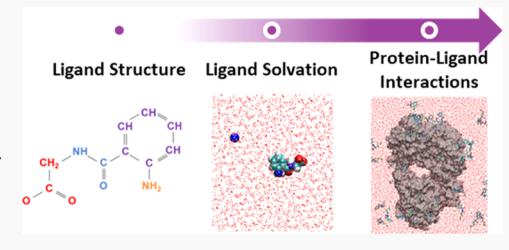
**ACCESS** I

Metrics & More



Supporting Information

**ABSTRACT:** Multimodal chromatography is a powerful approach for purifying proteins that uses ligands containing multiple modes of interaction. Recent studies have shown that selectivity in multimodal chromatographic separations is a function of the ligand structure and geometry. Here, we performed molecular dynamics simulations to explore how the ligand structure and geometry affect ligand—water interactions and how these differences in solution affect the nature of protein—ligand interactions. Our investigation focused on three chromatography ligands: Capto MMC, Nuvia cPrime, and Prototype 4, a structural variant of Nuvia cPrime. First, the solvation characteristics of each ligand were quantified via three



metrics: average water density, fluctuations, and residence time. We then explored how solvation was perturbed when the ligand was bound to the protein surface and found that the probability of the phenyl ring dewetting followed the order: Capto MMC > Prototype 4 > Nuvia cPrime. To explore how these differences in dewetting affect protein—ligand interactions, we calculated the probability of each ligand binding to different types of residues on the protein surface and found that the probability of binding to a hydrophobic residue followed the same order as the dewetting behavior. This study illustrates the role that wetting and dewetting play in modulating protein—ligand interactions.

# **■ INTRODUCTION**

In recent years, protein-based therapeutics have emerged as a powerful approach to treating complex diseases, fueling the need for developing effective and efficient methods for purifying these drugs at scale. Recently, a new type of chromatography, multimodal chromatography, has emerged as a leading approach for performing protein separations.<sup>1,2</sup> Unlike single-mode chromatography techniques, multimodal chromatography separates proteins by using ligands capable of multiple types of weak interactions (e.g., charge, hydrophobicity, and hydrogen bonding). By combining these modes of interaction synergistically, ligands can bind with varying affinities to proteins that differ by only small changes in their surface properties.<sup>3,4</sup> This has made multimodal chromatography particularly effective at purifying difficult-to-separate, industrially relevant mixtures such as product-related variants and aggregate species. 1,5-7 Despite these advantages, the promise of multimodal chromatography in industrial applications has not been fully realized due to a poor fundamental understanding of the nature of protein-multimodal ligand interactions.

Protein—ligand interactions in multimodal chromatography are complex in nature. The protein and the ligand-covered resin surface interact with each other through many types of noncovalent interactions, each of which are mediated by water and ions. Many studies have attempted to simplify this problem by assuming that weak multimodal interactions are additive in nature. While this assumption can prove useful in specific circumstances, many studies have shown that even

most commonly used multimodal ligands display nonadditive behavior when interacting with therapeutically relevant proteins.<sup>3</sup> In fact, Woo et al.<sup>10,11</sup> and Robinson et al.<sup>12,13</sup> illustrated that multimodal resins with different chemistries and architectures lead to changes in selectivity and Bilodeau et al.<sup>14</sup> showed that multimodal resins are generally orthogonal to ion exchange resins. Thus, this nonadditive behavior is not an exception but rather the norm.<sup>15</sup>

The nonadditivity of multimodal interactions is not unique to protein separations and has been observed in many other biological and colloidal systems. Recent studies indicate that the hydrophobic effect near molecules and at interfaces is governed by the density fluctuations and dynamics of water molecules. <sup>16–19</sup> The behavior of these water molecules is, in turn, governed not only by the presence of specific chemical groups but also by the precise arrangement and patterning of those chemical groups. <sup>20–22</sup> This phenomenon has implications for a variety of important systems including protein—drug interactions. <sup>23,24</sup> and protein—protein interactions. <sup>17,25</sup>

Molecular dynamics (MD) simulations have been previously used to fundamentally understand molecular-scale phenomena

Recived: February 22, 2021 Revised: May 20, 2021 Published: June 7, 2021





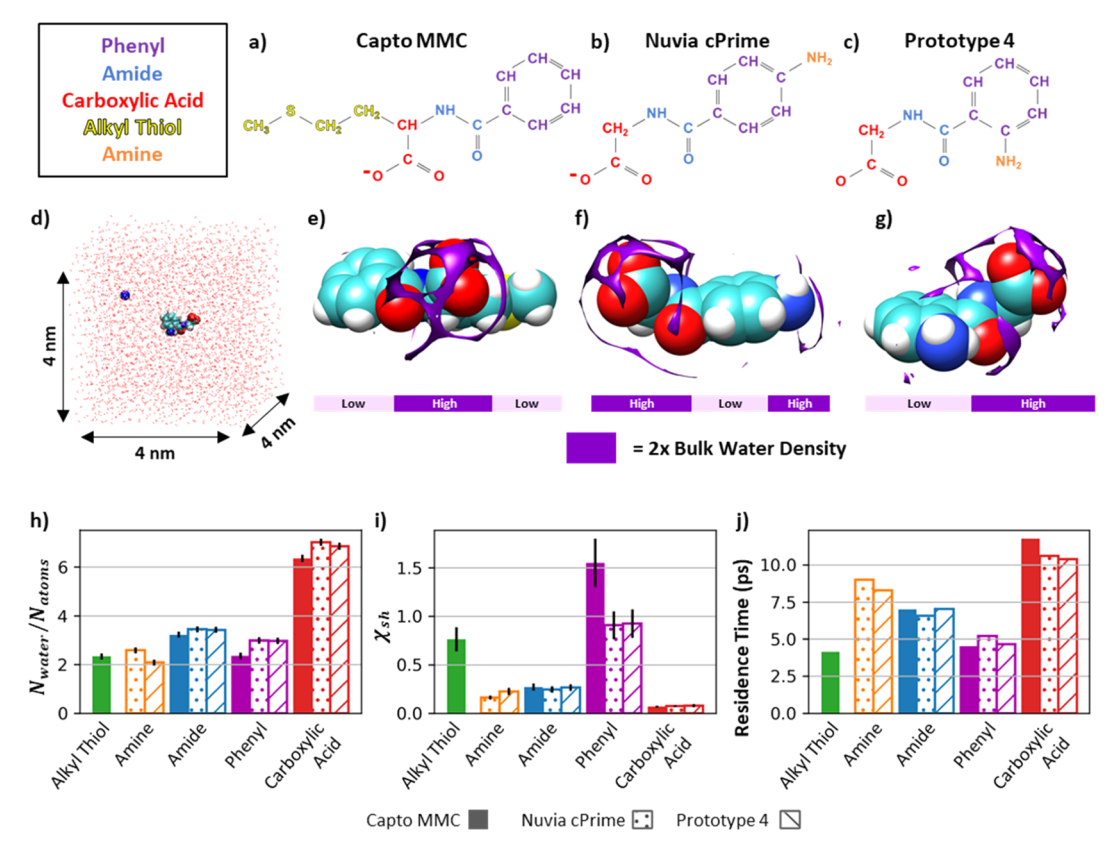


Figure 1. (a-c) Chemical structures of Capto MMC, Nuvia cPrime, and Prototype 4, respectively, with the color representing the type of chemical moiety. (d) Snapshot from an MD simulation of Prototype 4 and a sodium counterion (spacefill) solvated in water (wireframe) in a three-dimensional periodic box with dimensions of  $\sim$ 4 × 4 × 4 nm. Color scheme: sodium, blue; hydrogen, white; oxygen, red; carbon, cyan; and nitrogen, blue. (e-g) Spatial density distribution function of water near Capto MMC, Nuvia cPrime, and Prototype 4, respectively, with a purple contour representing the water density equal to 2× the bulk water density. (h) Number of water molecules in the solvation shell of each moiety normalized by the number of heavy atoms present in that moiety for Capto MMC (solid), Nuvia cPrime (dotted), and Prototype 4 (hashed). (i) Fluctuations in the number of water molecules in the solvation shell of each moiety normalized by the number of atoms present in that moiety for Capto MMC (solid), Nuvia cPrime (dotted), and Prototype 4 (hashed). (j) Average water residence time for each moiety for Capto MMC (solid), Nuvia cPrime (dotted), and Prototype 4 (hashed).

in chromatographic systems. MD simulations have been successfully applied in identifying protein binding orientation and conformation in ion exchange, hydrophobic charge induction, and multimodal chromatography. 26-29 Additionally, the simulations have yielded insights into the mechanism by which arginine can elute proteins from Protein A, 30,31 multimodal cation exchange, and multimodal anion exchange resins. 30,31 Finally, the technique can be used to identify binding free energies of specific protein faces,<sup>32</sup> and when combined with molecular mechanics/Poisson-Boltzmann solvent accessible surface area methods shows potential for predicting the relative free energy of binding to chromatographic surfaces. 33,34 Here, we focus on the role that water plays in governing protein-ligand interactions, a perspective that has proven useful for understanding protein folding<sup>35,36</sup> and protein-protein interactions, 18,37 but which has been less thoroughly explored for chromatographic applications.

In this paper, we explore the role that chemistry and chemical arrangement play in governing the hydrophobicity of three multimodal cation exchange ligands. We first study the water behavior near each ligand by performing MD simulations and analyzing the average water density distribution, the water fluctuations in the ligand solvation shell, and the water residence time in the ligand solvation shell. We then perform simulations with ligands in free solution around the protein to

investigate how water behavior changes when the ligand binds to the protein surface. Finally, we explore how these differences in water behavior drive differences in ligand affinity for various types of amino acids. This investigation illustrates how changes in ligand chemistry and architecture cause changes in solvation which, in turn, govern ligand—protein interactions.

# METHODS

As has been described previously,<sup>38</sup> Capto MMC (Cytiva) and Nuvia cPrime (Bio-Rad Laboratories) are both commonly used, commercially available multimodal cation-exchange ligands (Figure 1a,b). Prototype 4, a ligand based off of the structure of Nuvia cPrime, was developed previously in a collaboration with Bio-Rad<sup>11</sup> and differs from Nuvia cPrime in that the amine is located at the ortho position instead of the para position, as shown in Figure 1c. In the chromatographic resin, Capto MMC is immobilized to an agarose bead via a polyglycerol linker attached to the alkyl thiol group (yellow), while Nuvia cPrime and Prototype 4 are both immobilized directly to a polyacrylamide bead via the amine group (orange). In this study, we explore the behavior of water molecules near each ligand by performing MD simulations of each ligand alone in water and in the presence of three antibody fragments.

Single Ligand in Water. MD simulations first were performed with each ligand solvated in a 4 nm cubic box of TIP4P water with a single sodium counterion. <sup>39,40</sup> A previous work showed that ligand hydration and conformational behavior are similar for TIP3P and TIP4P force fields.<sup>38</sup> The general Amber force field<sup>41</sup> was used to assign force-field parameters to each ligand and the RESP method<sup>42</sup> was used to assign partial charges, as has been described previously (parameters for Prototype 4 can be found in Supporting Information because they have not been previously reported).<sup>38</sup> Simulations were performed using GROMACS 4.5.3<sup>43-45</sup> for 10 ns with a timestep of 2 fs and storing coordinates every 1 ps. Bonds with hydrogen atoms were constrained using LINCS. 46 The Particle-Mesh Ewald method<sup>47</sup> with a 0.1 nm grid was used to calculate electrostatics. Simulations were performed in the NPT ensemble with a temperature of 298 K and a pressure of 1 bar achieved using a Nosé-Hoover thermostat<sup>48</sup> and a Parrinello-Rahman barostat, 49 respectively.

Ligands in the Presence of Proteins. To explore how ligands are hydrated during the binding/unbinding process in proteins, each ligand was then simulated in free solution around three Fab fragments from different antibodies referred to here as Fabs A, B, and C (9 simulations total). Each simulation included 64 ligand molecules (~0.1 M concentration), 64 sodium counterions, and one protein and was solvated in TIP3P water molecules<sup>39</sup> to fill a box size of 9.5 ×  $10 \times 12$  nm (selected to allow for a margin of  $\sim 1.5$  nm on each side of the protein). Each protein was modeled using the AMBER99 force field<sup>50</sup> and the protonation states of the side chains were determined using PROPKA<sup>51</sup> at pH 6 which is a typical pH for preparative multimodal cation exchange separations. Four buried alpha carbons near the center of each domain of each Fab were harmonically constrained with a 40,000 kJ/(mol·nm<sup>2</sup>) to prevent translation and rotation of the protein. All other MD parameters remained unchanged.

Spatial Density Distribution Function Calculation. The spatial density distribution function for each ligand was calculated by first performing hierarchical clustering over the ligand conformation (based on torsion angle) in each frame of the MD trajectory containing only a ligand in water. The centroid of the largest cluster was then used as the conformation for calculating the spatial density distribution function. An additional 1 ns MD simulation was performed with the ligand heavy atoms harmonically constrained with a constant of 40,000 kJ/(mol·nm²). Average water density near the ligand was then calculated from this 1 ns trajectory at each point on a cubic grid centered around the ligand with side length 2.5 and 0.1 nm spacing.

Average Residence Time Distribution Calculation. The average water residence time is the average quantity of time the water spends in the solvation shell of a given atom. Because this phenomenon occurs on a shorter timescale than the other behaviors studied, an additional 1 ns simulation was performed saving frames every 0.01 ps (for a total of 11 ns simulation time). Any average residence times reported are calculated only on this last 1 ns and all other reported measurements are calculated only on the first 10 ns. We then consider water molecules to be in the solvation shell of a given heavy atom if the oxygen atom is within 0.4 nm of the atom. To account for water molecules lingering near this threshold, we use a buffer time of 0.1 ps such that if the water molecule

leaves but comes back within 0.1 ps the water molecule is considered to have never left.

## ■ RESULTS AND DISCUSSION

Our investigation focused on three multimodal cation exchange chromatography ligands. Two of these, Capto MMC and Nuvia cPrime, are commonly used, commercially available ligands. The third ligand, Prototype 4, was previously developed in collaboration with Bio-Rad and is based on the structure of Nuvia cPrime. Each ligand contains a common chemical motif (hippuric acid) consisting of a phenyl ring connected to a carboxylate by an amide linker, making each ligand negatively charged and partially hydrophobic. In addition, Capto MMC has an alkyl thiol group attached to the methylene portion of hippuric acid and Nuvia cPrime has an amine group bonded to the phenyl ring at the para position. Prototype 4 differs from Nuvia cPrime in that the amine group is instead located at the ortho position.

Despite the fact that these three ligands had nearly identical chemistry, multiple studies have shown that their subtle differences in the structure can lead to significant changes in selectivity. In particular, comparisons between Capto MMC and Nuvia cPrime on libraries of model proteins, 10 Fab variants,<sup>53</sup> and mAbs<sup>12</sup> showed that Capto MMC strongly retained proteins with exposed hydrophobic regions, in some cases leading to greater selectivity on the basis of hydrophobicity. Prototype 4 (ortho configuration) has also been shown to have enhanced retention of proteins compared with Nuvia cPrime and in different cases has had selectivities resembling either Capto MMC or Nuvia cPrime. 11,12 This leads to the question: How do subtle molecular differences between multimodal ligands lead to significant changes in protein-ligand interactions? The first part of this paper studies how small molecular perturbations cause differences in molecular solvation. The second part of this paper explores how these differences in solvation lead to differences in protein-ligand interactions.

**Ligand–Water Interactions.** The strength of water-mediated protein–ligand interactions results from a balance between direct protein–ligand, protein–water, and ligand–water interactions.<sup>38</sup> Therefore, to understand how ligands differ in terms of protein selectivity, it is important to first study how ligand–water interactions are controlled by ligand chemistry. We evaluated the solvation characteristics of each ligand by performing MD simulations in a 64 nm<sup>3</sup> cubic box with a single counterion (Figure 1d) and measured three attributes of water behavior in the solvation shells of the ligands as follows: density at equilibrium, density fluctuations, and residence time.

Figure 1e—g illustrates the water density at equilibrium in the vicinity of Capto MMC, Nuvia cPrime, and Prototype 4, through visualizing the spatial density distribution function of water as a purple isosurface representing water density greater than twice that of bulk water. As expected, high-density regions of water were found to occur near the hydrogen bonding groups on each ligand. For Capto MMC (Figure 1e), the hydrogen bonding groups (the carboxylate and amide groups) were located near the center of the ligand, while the relatively hydrophobic moieties formed the two ends of the ligand. In contrast, Nuvia cPrime's hydrogen bonding groups (the carboxylate, amide, and amine groups) were located at the ends of the ligand with the comparatively hydrophobic region centered toward the middle of the ligand (Figure 1f). In this

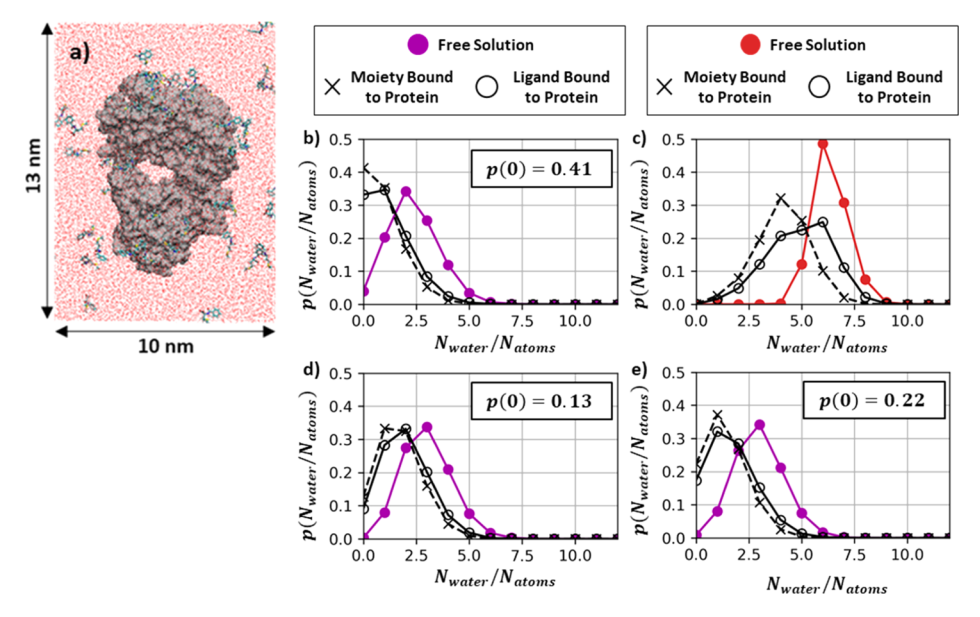


**Figure 2.** (a) Snapshot from an MD simulation of Fab A (gray, surface representation) solvated in water (wireframe) with Capto MMC ligands (licorice). Color scheme: hydrogen, white; oxygen, red; carbon, cyan; and nitrogen, blue. Probability of observing  $N_{\text{water}}$  molecules in the solvation shell of (b) phenyl ring of Capto MMC, (c) carboxylate of Capto MMC, (d) phenyl ring of Nuvia cPrime, and (e) phenyl ring of Prototype 4 in a free solution (colored purple for the phenyl ring and red for the carboxylate), with the ligand bound to the protein (black open circles) and the moiety bound to the protein (black, dashed line, x markers).

way, water density near Capto MMC followed a "low-high-low" motif, while the water density near Nuvia cPrime followed a "high-low-high" motif. This difference in solvation likely affects the nature of protein—ligand interactions in solution because the ends of each ligand are more accessible to the protein than the ligand center. As described earlier, Prototype 4 differed from Nuvia cPrime in that the amine was located at the ortho instead of the para position. Figure 1g illustrates that this difference caused the water density near the amine to merge with the water density near the amide/carboxylate groups, leading to a "low-high" water density motif.

Figure 1h illustrates the equilibrium water density in the solvation shell of each moiety within each ligand. The carboxylate on each ligand contained the most water molecules in its solvation shell, likely due to its ability to hydrogen bond with water at two locations. The amide group had the next highest number of water molecules in its solvation shell likely because it was capable of hydrogen bonding but was less sterically accessible. The phenyl and amine groups had similar numbers of water molecules in their solvation shells, likely because the water density on average near the amine was significantly affected by the much larger neighboring phenyl ring. Each type of chemical moiety had a relatively constant number of water molecules in its solvation shell across all three ligands, with only minor differences. The carboxylate and amine groups on Prototype 4 had fewer water molecules in their solvation shells compared to the same groups on Nuvia cPrime. We note that the amine group on Prototype 4 was found to hydrogen bond with the amide group, which is likely the reason for the reduced number of neighboring water molecules. In addition, the carboxylate, phenyl, and amide groups on Capto MMC had fewer water molecules in their solvation shells compared to the same groups on either Prototype 4 or Nuvia cPrime.

While the distribution of water density sheds light on the strength of ligand—water interactions, the free energy of forming a cavity in water near the ligand is more closely related

to fluctuations in water density. <sup>17,54</sup> In fact, numerous studies have shown that density fluctuations of water capture the macroscopic "contact-angle" notion of hydrophobicity better than water density and that, for a variety of common surfaces, equilibrium density and density fluctuations are not correlated. <sup>16,20</sup> Therefore, when studying ligand—water interactions, it is useful to not only measure equilibrium density but also density fluctuations.

Figure 1i illustrates the equilibrium water density fluctuations in the solvation shell of each moiety within each ligand normalized by the square of the average number of water molecules and the number of atoms in the moiety:

$$\chi_{\rm sh} = n_{\rm atoms} \frac{\langle n_{\rm water}^2 \rangle - \langle n_{\rm water} \rangle^2}{\langle n_{\rm water} \rangle^2}$$

where  $n_{\rm atoms}$  refers to the number of atoms in the moiety. Interestingly, the density fluctuations of water molecules in the solvation shell of the Capto MMC phenyl ring (purple, solid) were far higher than the phenyl rings of either Nuvia cPrime (purple, dotted) or Prototype 4 (purple, hashed), suggesting that the presence of the vicinal amine group dramatically affected the hydrophobicity of the phenyl ring. Additionally, while the equilibrium water densities in the solvation shell of the phenyl and amine groups were found to be similar, the water density fluctuations in the solvation shell of the phenyl ring were significantly higher than those near the amine group. Thus, while the amine group was solvated by relatively few water molecules, these molecules would be difficult for a protein to displace upon binding.  $^{55}$ 

While the equilibrium water density and the fluctuations about that equilibrium tell us about the thermodynamics of ligand—water interactions, they lack the time dependence required to describe the dynamics of the solvation shell water molecules. Water dynamics in the form of residence time and diffusivity have been shown to be exploited by biomolecules to affect functional dynamics. ST,58 Similarly, water dynamics near

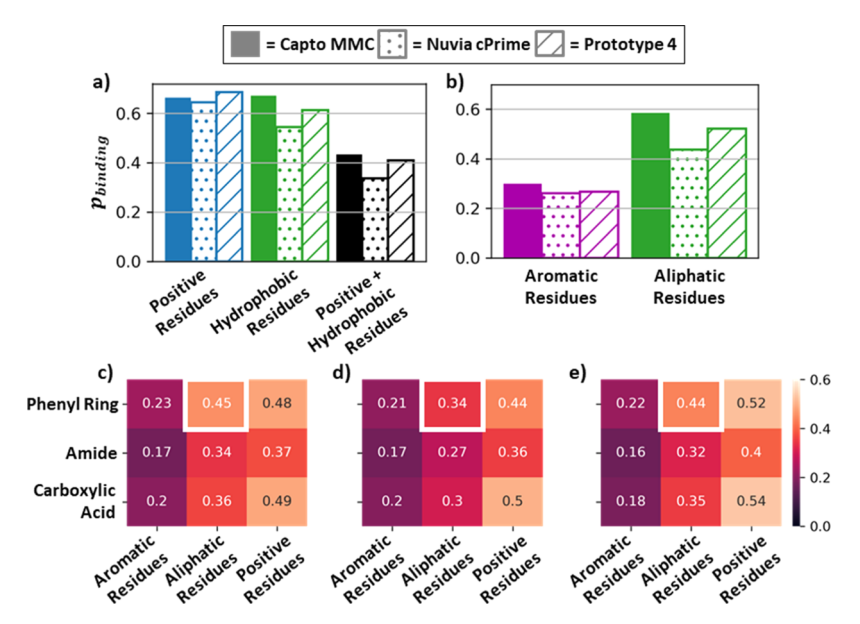


Figure 3. (a) Given the probability that each ligand is bound to the protein surface, the probability of each ligand to bind to a positively charged residue (blue), a hydrophobic residue (green), or a positively charged and hydrophobic residue simultaneously (black). (b) Given the probability that each ligand is bound to the protein surface, the probability of each ligand to be bound to an aromatic residue (purple) or an aliphatic residue (green). (c–e) Joint probability for Capto MMC, Nuvia cPrime, and Prototype 4, respectively; given that each ligand is bound to the protein surface, that a given moiety and residue are also involved in the binding interaction.

chromatography ligands on the timescale of adsorption/desorption events could influence water-mediated protein—ligand interactions.

To explore these water dynamics, Figure 1j illustrates the average residence time of water in the solvation shell of each atom in each moiety. As was observed for the previous two measurements, hydrogen bonding interactions drove the overall trends such that the highest residence times were observed for the carboxylate group. The alkyl thiol and phenyl rings, which did not hydrogen bond with water, had the lowest residence times. Interestingly, in contrast to the previous two measurements, water molecules in the solvation shell of the amine group had a higher residence time than in the solvation shell of the amide group. Thus, while strong ligand-water interactions tend to lead to high water density, low density fluctuations, and long water residence time, these measurements are not always correlated and therefore have different implications for quantifying the hydrophobic qualities of a given ligand.

Changes in Ligand—Water Interactions upon Binding to Proteins. To study how ligand—water interactions change when the ligand binds to the surface of a protein, we performed MD simulations of each ligand in free solution around three proteins, as illustrated in Figure 2a. We focused our study on three Fab fragments—referred to here as Fabs A, B, and C—of different antibodies that were representative of therapeutically relevant proteins. Each protein had different distributions of hydrophobic, polar, and charged patches as has been described previously. We performed 200 ns simulations, allowing each ligand to bind to each protein in a variety of chemical and topological settings and selected frames every 50 ps to evaluate ligand solvation. In this study, a ligand was considered bound if any heavy atom was located within 3 Å of any protein heavy atom.

Figure 2b shows the distribution of the number of water molecules in the solvation shell of the phenyl group for Capto MMC, normalized by the number of heavy atoms in the phenyl

group. In free solution, the probability of fully desolvating the phenyl group, p(0), was small (although nonzero). Upon binding to the protein surface, this probability increased dramatically, and given that the phenyl group was in contact with the protein (shown with x markers in Figure 2b), the probability of fully desolvating the phenyl group was 0.41. In contrast, the probability of fully desolvating the Capto MMC carboxylate (Figure 2c) was zero regardless of whether the ligand is bound or unbound.

Figure 2d shows the distribution of the number of water molecules in the solvation shell of Nuvia cPrime's phenyl group. In contrast to Capto MMC, upon binding to the protein surface, the probability of fully desolvating the Nuvia cPrime phenyl group remained comparatively low (0.13). Thus, while the Capto MMC phenyl group underwent full dewetting upon binding to the surface, the Nuvia cPrime phenyl group displayed only partial dewetting behavior. This is consistent with our observations of the individual Capto MMC and Nuvia cPrime ligands in aqueous solution, namely, that the Nuvia cPrime phenyl ring had higher water density, lower water fluctuations, and a higher water residence time when compared with the Capto MMC phenyl ring. The difference in the solvation characteristics of the two phenyl rings is likely due to the fact that the amine (located at the para position of the phenyl ring on Nuvia cPrime) was more difficult to desolvate than the phenyl rings, illustrated by the higher water densities, lower water fluctuations, and higher water residence times of the amine group compared to any of the phenyl rings (Figure

Figure 2e shows the distribution of the number of water molecules in the solvation shell of Prototype 4's phenyl group. Interestingly, upon binding to the protein surface, the Prototype 4 phenyl group displayed an intermediate probability of full desolvation [p(0) = 0.22]. Thus, shifting the location of the amine from the para position to ortho position increased the dewetting behavior of the phenyl ring, nearly doubling the probability of full dewetting. Unlike the

previous solvation trends, this intermediate dewetting behavior was not indicated by most of the measurements of the individual ligands. As shown in Figure 1h—j, the average water density, fluctuations, and residence time in the vicinity of the Prototype 4 phenyl ring did not differ significantly from the Nuvia cPrime phenyl ring. This is likely because the increase in dewetting can be attributed to the improved accessibility of the phenyl ring, illustrated by the "low-high" motif observed in Figure 1g, allowing the phenyl ring to readily bind to the protein unimpeded by the amine group.

Ligand-Residue Interaction Preferences. In the previous sections, we have investigated how water solvates Capto MMC, Nuvia cPrime, and Prototype 4 ligands in free solution and bound to the surfaces of proteins. How do changes in solvation drive differences in selectivity for proteins with varying surface properties? To address this question, Figure 3a shows the probability of each ligand binding to a given type of residue (normalized by the probability that the ligand was bound to the protein). While each ligand was roughly equally likely to bind to a positively charged residue (blue), there were significant differences in each ligands' propensity to bind to a hydrophobic residue (green). As can be seen, while Capto MMC was the most likely to bind to a hydrophobic residue, Nuvia cPrime was the least likely. Interestingly, Prototype 4 exhibited an intermediate probability of binding to the hydrophobic residues. We also found that Capto MMC and Prototype 4 were roughly equally likely to bind simultaneously to both positively charged and hydrophobic residues, while Nuvia cPrime was less likely to do so. This difference was largely driven by the tendency for Capto MMC and Nuvia cPrime to interact with aliphatic residues as compared to Nuvia cPrime (Figure 3b). This is consistent with the prior work reported by Parimal et al.<sup>59</sup> where it was found that for two proteins, ubiquitin and  $\alpha$ -chymotrypsinogen A, Capto MMC tended to interact strongly with aliphatic clusters on the protein surface while Nuvia cPrime interacted relatively

To explore how the observed differences in protein—ligand interactions could be attributed to differences in the ligand structure, Figure 3c—e illustrates the joint probability of each moiety in the ligands binding to each residue type considered for Capto MMC, Nuvia cPrime, and Prototype 4, respectively (again normalized by the probability that each ligand was bound to the protein). While most of these joint probabilities were similar across all three ligands, the joint probability that the phenyl ring and aliphatic residues were involved in binding was significantly higher for Capto MMC and Prototype 4 (0.45 and 0.44, respectively) as compared with the Nuvia cPrime ligand (0.34). This illustrates that the observed preference for aliphatic residues by Capto MMC and Prototype 4 in comparison with Nuvia cPrime can be attributed to differences in the behavior of the phenyl ring.

These differences in ligand—residue interactions can lead to differences in the relative strength of interactions as well as the shapes, sizes, and positions of the preferred binding regions on the proteins. To illustrate this, Figure 4 shows the specific case of these ligands binding to the proximal positively charged (colored blue in Figure 4) and hydrophobic regions (including aromatic and aliphatic residues, colored purple and green, respectively, in Figure 4) in the complementary-determining region (CDR) of Fab C. While all three ligands bound to the positively charged region (illustrated by the black, mesh isosurface in Region 1 in Figure 4), Capto MMC bound to a

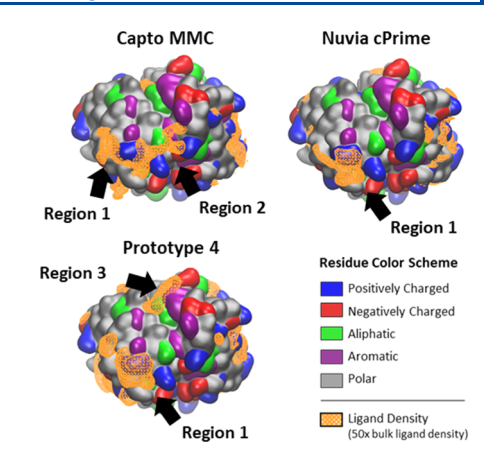


Figure 4. Snapshots of the top (CDR) of Fab C, represented using a surface representation and colored based on residue type: aromatic, purple; positively charged, blue; negatively charged, red; aliphatic, green; and polar, gray. Ligand density is shown as an orange mesh contour representing a bound density of 50× bulk ligand density.

wider region, also encompassing the hydrophobic residues (Region 2 in Figure 4). While Prototype 4 was not observed to bind to the hydrophobic region in the center of the CDR loops (Region 2 in Figure 4), it did interact favorably with a second, separate hydrophobic region in the CDR (Region 3 in Figure 4). Thus, the differences in each ligands' interaction with the different residue types resulted in each ligand interrogating a different combination of regions on the protein surface.

## CONCLUSIONS

In this work, we performed MD simulations to explore how multimodal ligand solvation and desolvation govern proteinligand interactions. We first quantified the average water density, fluctuations, and residence time near each ligand and found that small differences in the ligand arrangement affected how water molecules behaved in the solvation shell of each ligand. These differences in solvation were then found to drive differences in dewetting upon each ligand binding to the surface of a protein, such that that the Capto MMC phenyl ring had a high probability of fully dewetting (0.41), the Prototype 4 phenyl ring had an intermediate probability of fully dewetting (0.22), and the Nuvia cPrime phenyl ring had a low probability of fully dewetting (0.13). These solvation/ desolvation trends affected how each ligand interacted with different types of residues on the protein surface. While each ligand was bound to positively charged residues with a roughly equal probability, the probability of binding to a hydrophobic residue followed the order Capto MMC > Prototype 4 > Nuvia cPrime, matching the order of the probability of full desolvation. These differences in ligand-residue interactions resulted in the formation of different protein-ligand interaction hotspots, illustrated in Figure 4. This work illustrates how a small modification to Nuvia cPrime such as changing the phenyl ring substitution can dramatically change ligand solvation, which in turn affects protein-ligand interactions.

The dewetting behavior of these ligands also has important implications for understanding previously reported experimental trends. Woo et al. 10 showed that a library of model proteins was generally more retained on Capto MMC compared with Nuvia cPrime. They also showed that proteins with particularly enhanced retention on Capto MMC were classified as

aliphatic, while proteins that were highly retained on both resins were aromatic. Similarly, Woo et al. 11 showed that Prototype 4 retained proteins more strongly than Nuvia cPrime and attributed this to the increase in hydrophobic surface area associated with the change in the phenyl ring substitution. More recently, Gudhka et al. 60 showed that Capto MMC has a more hydrophobic character than Nuvia cPrime by performing isocratic experiments with two mAbs at varying salt concentrations. The results reported in this article are qualitatively consistent with these previous experimental findings and illustrate the potential underlying molecular phenomena that drive the observed chromatographic behavior.

Here, we presented a workflow for quantifying ligand solvation properties and illustrated that these properties are important for describing protein-ligand interactions. While simulating proteins in the presence of ligands (the last two sections) is computationally expensive, it is relatively inexpensive to simulate individual ligands in water and measure solvation characteristics. Therefore, in the future, we will use these measurements as quick screening metrics that can be easily used to evaluate which new ligand designs have the potential to have interesting selectivities. Further, for systems where experimental data are available, we will use these properties as QSAR descriptors<sup>11</sup> and evaluate their ability to predict protein retention in a chromatography column. In this way, we envision that ligands deemed promising using molecular simulations and/or other modeling techniques could then be synthesized and tested experimentally.

While in this work, we have focused on ligands interacting with proteins in free solution, in a chromatography column, ligands are immobilized on a resin surface. In this context, ligands are forced to remain in close proximity to one another, which at relevant ligand densities can result in the formation of ligand aggregates near the resin surface. 61 Therefore, in the future, we will explore the solvation characteristics of ligands immobilized on a surface. It is important to note that while the properties of the chromatographic surface are likely to be of great importance to understanding selectivity in multimodal chromatography, they will also be more challenging to study. Because multimodal surfaces are large, soft, and flexible and the solvation shell is difficult to define, enhanced sampling techniques will likely be required to accurately evaluate water behavior. Therefore, we believe that these two levels of complexity, free ligand simulations (less complex) and surfaceimmobilized ligand simulations (more complex), should be used in a strategic combination to further explore proteinligand interactions in multimodal chromatographic systems.

## ASSOCIATED CONTENT

## Supporting Information

The Supporting Information is available free of charge at https://pubs.acs.org/doi/10.1021/acs.jpcb.1c01549.

Prototype 4 topology and structure information (PDF)

#### AUTHOR INFORMATION

# **Corresponding Author**

Camille L. Bilodeau – Howard P. Isermann Department of Chemical and Biological Engineering and Center for Biotechnology and Interdisciplinary Studies, Rensselaer Polytechnic Institute, Troy, New York 12180, United States; Department of Chemical Engineering, Massachusetts Institute of Technology, Cambridge, Massachusetts 02139, United States; orcid.org/0000-0002-8358-5280; Email: cbilod@mit.edu

## **Authors**

Edmond Y. Lau – Physical and Life Sciences Directorate, Lawrence Livermore National Laboratory, Livermore, California 94550, United States

David J. Roush – Biologics Process R&D, Merck & Co., Inc., Kenilworth, New Jersey 07033, United States

Mark A. Snyder – Process Chromatography Division, Bio-Rad Laboratories, Hercules, California 94547, United States

Steven M. Cramer — Howard P. Isermann Department of Chemical and Biological Engineering and Center for Biotechnology and Interdisciplinary Studies, Rensselaer Polytechnic Institute, Troy, New York 12180, United States; orcid.org/0000-0003-4993-0826

Complete contact information is available at: https://pubs.acs.org/10.1021/acs.jpcb.1c01549

#### **Notes**

The authors declare no competing financial interest.

#### ACKNOWLEDGMENTS

We gratefully acknowledge discussions with Dr. Shekhar Garde. This material is based upon work partially supported by the National Science Foundation under grant no. (CBET 1704745) as well as the ASC Graduate Fellowship Program (Lawrence Livermore National Laboratory), Merck & Co., Inc. (Kenilworth, NJ, 07033, USA), and Bio-Rad laboratories (Hercules, CA, 94547, USA). Work at the Lawrence Livermore National Laboratory (LLNL) was performed under the auspices of the U.S. Department of Energy by Lawrence Livermore National Laboratory under contract DE-AC52-07NA27344.

#### REFERENCES

- (1) Halan, V.; Maity, S.; Bhambure, R.; Rathore, A. S. Multimodal Chromatography for Purification of Biotherapeutics A Review. *Curr. Protein Pept. Sci.* **2018**, *20*, 4–13.
- (2) Cramer, S. M.; Holstein, M. A. Downstream Bioprocessing: Recent Advances and Future Promise. *Curr. Opin. Chem. Eng.* **2011**, *1*, 27–37.
- (3) Karkov, H. S.; Krogh, B. O.; Woo, J.; Parimal, S.; Ahmadian, H.; Cramer, S. M. Investigation of Protein Selectivity in Multimodal Chromatography Using in Silico Designed Fab Fragment Variants. *Biotechnol. Bioeng.* **2015**, *112*, 2305–2315.
- (4) Holstein, M. A.; Chung, W. K.; Parimal, S.; Freed, A. S.; Barquera, B.; McCallum, S. A.; Cramer, S. M. Probing Multimodal Ligand Binding Regions on Ubiquitin Using Nuclear Magnetic Resonance, Chromatography, and Molecular Dynamics Simulations. *J. Chromatogr.* **2012**, *1229*, 113–120.
- (5) Zhang, L.; Parasnavis, S.; Li, Z.; Chen, J.; Cramer, S. Mechanistic Modeling Based Process Development for Monoclonal Antibody Monomer-Aggregate Separations in Multimodal Cation Exchange Chromatography. *J. Chromatogr. A* **2019**, *1602*, 317–325.
- (6) Vecchiarello, N. A. In Silico Design of Integrated Chromatographic Purification Processes for Therapeutic Proteins; Wiley: Troy, NY, 2019.
- (7) Chmielowski, R. A.; Meissner, S.; Roush, D.; Linden, T. O.; Glowacki, E.; Konietzko, J.; Nti-Gyabaah, J. Resolution of Heterogeneous Charged Antibody Aggregates via Multimodal Chromatography: A Comparison to Conventional Approaches. *Biotechnol. Prog.* **2014**, *30*, 636–645.
- (8) Pinto, I. F.; Soares, R. R. G.; Rosa, S. A. S. L.; Aires-Barros, M. R.; Chu, V.; Conde, J. P.; Azevedo, A. M. High-Throughput

- Nanoliter-Scale Analysis and Optimization of Multimodal Chromatography for the Capture of Monoclonal Antibodies. *Anal. Chem.* **2016**, *88*, 7959–7967.
- (9) Nfor, B. K.; Noverraz, M.; Chilamkurthi, S.; Verhaert, P. D. E. M.; van der Wielen, L. A. M.; Ottens, M. High-Throughput Isotherm Determination and Thermodynamic Modeling of Protein Adsorption on Mixed Mode Adsorbents. *J. Chromatogr.* **2010**, *1217*, 6829–6850.
- (10) Woo, J.; Parimal, S.; Brown, M. R.; Heden, R.; Cramer, S. M. The Effect of Geometrical Presentation of Multimodal Cation-Exchange Ligands on Selective Recognition of Hydrophobic Regions on Protein Surfaces. *J. Chromatogr.* **2015**, *1412*, 33–42.
- (11) Woo, J. A.; Chen, H.; Snyder, M. A.; Chai, Y.; Frost, R. G.; Cramer, S. M. Defining the Property Space for Chromatographic Ligands from a Homologous Series of Mixed-Mode Ligands. *J. Chromatogr.* **2015**, *1407*, 58–68.
- (12) Robinson, J.; Roush, D.; Cramer, S. Domain Contributions to Antibody Retention in Multimodal Chromatography Systems. *J. Chromatogr.* **2018**, *1563*, 89–98.
- (13) Robinson, J.; Snyder, M. A.; Belisle, C.; Liao, J.-l.; Chen, H.; He, X.; Xu, Y.; Cramer, S. M. Investigating the Impact of Aromatic Ring Substitutions on Selectivity for a Multimodal Anion Exchange Prototype Library. *J. Chromatogr. A* **2018**, *1569*, 101–109.
- (14) Bilodeau, C. L.; Vecchiarello, N. A.; Altern, S.; Cramer, S. M. Quantifying Orthogonality and Separability: A Method for Optimizing Resin Selection and Design. *J. Chromatogr. A* **2020**, *1628*, 461429.
- (15) Brown, M. R.; Burnham, M. S.; Lute, S. C.; Johnson, S. A.; Walsh, A. A.; Brorson, K. A.; Roush, D. J. Defining the Mechanistic Binding of Viral Particles to a Multi-Modal Anion Exchange Resin. *Biotechnol. Prog.* **2018**, *34*, 1019–1026.
- (16) Godawat, R.; Jamadagni, S. N.; Garde, S. Characterizing Hydrophobicity of Interfaces by Using Cavity Formation, Solute Binding, and Water Correlations. *Proc. Natl. Acad. Sci. U.S.A.* **2009**, *106*, 15119–15124.
- (17) Patel, A. J.; Varilly, P.; Jamadagni, S. N.; Hagan, M. F.; Chandler, D.; Garde, S. Sitting at the Edge: How Biomolecules Use Hydrophobicity to Tune Their Interactions and Function. *J. Phys. Chem. B* **2012**, *116*, 2498–2503.
- (18) Rego, N. B.; Xi, E.; Patel, A. J. Protein Hydration Waters Are Susceptible to Unfavorable Perturbations. *J. Am. Chem. Soc.* **2019**, 141, 2080–2086.
- (19) Monroe, J.; Barry, M.; DeStefano, A.; Aydogan Gokturk, P.; Jiao, S.; Robinson-Brown, D.; Webber, T.; Crumlin, E. J.; Han, S.; Shell, M. S. Water Structure and Properties at Hydrophilic and Hydrophobic Surfaces. *Annu. Rev. Chem. Biomol. Eng.* **2020**, *11*, 523–557.
- (20) Acharya, H.; Vembanur, S.; Jamadagni, S. N.; Garde, S. Mapping Hydrophobicity at the Nanoscale: Applications to Heterogeneous Surfaces and Proteins. *Faraday Discuss.* **2010**, *146*, 353–365.
- (21) Xi, E.; Venkateshwaran, V.; Li, L.; Rego, N.; Patel, A. J.; Garde, S. Hydrophobicity of Proteins and Nanostructured Solutes Is Governed by Topographical and Chemical Context. *Proc. Natl. Acad. Sci. U.S.A.* 2017, 114, 13345–13350.
- (22) Davis, J. G.; Zukowski, S. R.; Rankin, B. M.; Ben-Amotz, D. Influence of a Neighboring Charged Group on Hydrophobic Hydration Shell Structure. *J. Phys. Chem. B* **2015**, *119*, 9417–9422.
- (23) Rudling, A.; Orro, A.; Carlsson, J. Prediction of Ordered Water Molecules in Protein Binding Sites from Molecular Dynamics Simulations: The Impact of Ligand Binding on Hydration Networks. *J. Chem. Inf. Model.* **2018**, *58*, 350.
- (24) Wong, S. E.; Lightstone, F. C. Accounting for Water Molecules in Drug Design. *Expert Opin. Drug Discovery* **2011**, *6*, 65–74.
- (25) Pavlova, A.; Cheng, C.-Y.; Kinnebrew, M.; Lew, J.; Dahlquist, F. W.; Han, S. Protein Structural and Surface Water Rearrangement Constitute Major Events in the Earliest Aggregation Stages of Tau. *Proc. Natl. Acad. Sci. U.S.A.* **2016**, *113*, E127–E136.
- (26) Zhang, L.; Zhao, G.; Sun, Y. Molecular Insight into Protein Conformational Transition in Hydrophobic Charge Induction

- Chromatography: A Molecular Dynamics Simulation. *J. Phys. Chem.* B **2009**, 113, 6873–6880.
- (27) Zhang, L.; Bai, S.; Sun, Y. Molecular Dynamics Simulation of the Effect of Ligand Homogeneity on Protein Behavior in Hydrophobic Charge Induction Chromatography. *J. Mol. Graph. Model.* **2010**, *28*, 863–869.
- (28) Tong, H.-F.; Cavallotti, C.; Yao, S.-J.; Lin, D.-Q. Molecular Insight into Protein Binding Orientations and Interaction Modes on Hydrophobic Charge-Induction Resin. *J. Chromatogr. A* **2017**, *1512*, 34.
- (29) Zhang, L.; Sun, Y. Molecular Simulation of Adsorption and Its Implications to Protein Chromatography: A Review. *Biochem. Eng. J.* **2010**, *48*, 408–415.
- (30) Shukla, D.; Zamolo, L.; Cavallotti, C.; Trout, B. L. Understanding the Role of Arginine as an Eluent in Affinity Chromatography via Molecular Computations. *J. Phys. Chem. B* **2011**, *115*, 2645–2654.
- (31) Hirano, A.; Arakawa, T.; Kameda, T. Effects of Arginine on Multimodal Anion Exchange Chromatography. *Protein Expression Purif.* **2015**, *116*, 105–112.
- (32) Srinivasan, K.; Banerjee, S.; Parimal, S.; Sejergaard, L.; Berkovich, R.; Barquera, B.; Garde, S.; Cramer, S. M. Single Molecule Force Spectroscopy and Molecular Dynamics Simulations as a Combined Platform for Probing Protein Face-Specific Binding. *Langmuir* 2017, 33, 10851–10860.
- (33) Tong, H.-F.; Lin, D.-Q.; Zhang, Q.-L.; Wang, R.-Z.; Yao, S.-J. Molecular Recognition of Fc-Specific Ligands Binding onto the Consensus Binding Site of IgG: Insights from Molecular Simulation. *J. Mol. Recognit.* **2014**, *27*, 501–509.
- (34) Banerjee, S.; Parimal, S.; Cramer, S. M. A Molecular Modeling Based Method to Predict Elution Behavior and Binding Patches of Proteins in Multimodal Chromatography. *J. Chromatogr.* **2017**, *1511*, 45–58.
- (35) Zhou, R. Hydrophobic Collapse in Multidomain Protein Folding. *Science* **2004**, *305*, 1605–1609.
- (36) Liu, P.; Huang, X.; Zhou, R.; Berne, B. J. Observation of a Dewetting Transition in the Collapse of the Melittin Tetramer. *Nature* **2005**, 437, 159–162.
- (37) Giovambattista, N.; Lopez, C. F.; Rossky, P. J.; Debenedetti, P. G. Hydrophobicity of Protein Surfaces: Separating Geometry from Chemistry. *Proc. Natl. Acad. Sci. U.S.A.* **2008**, *105*, 2274–2279.
- (38) Bilodeau, C. L.; Lau, E. Y.; Cramer, S. M.; Garde, S. Conformational Equilibria of Multimodal Chromatography Ligands in Water and Bound to Protein Surfaces. *J. Phys. Chem. B* **2019**, *123*, 4833—4843
- (39) Jorgensen, W. L. Transferable Intermolecular Potential Functions for Water, Alcohols, and Ethers: Application to Liquid Water. J. Am. Chem. Soc. 1981, 103, 335–340.
- (40) Joung, I. S.; Cheatham, T. E. Molecular Dynamics Simulations of the Dynamic and Energetic Properties of Alkali and Halide Ions Using Water-Model-Specific Ion Parameters. *J. Phys. Chem. B* **2009**, 113, 13279–13290.
- (41) Wang, J.; Wolf, R. M.; Caldwell, J. W.; Kollman, P. A.; Case, D. A. Development and Testing of a General Amber Force Field. *J. Comput. Chem.* **2004**, *25*, 1157–1174.
- (42) Bayly, C. I.; Cieplak, P.; Cornell, W.; Kollman, P. A. A Well-Behaved Electrostatic Potential Based Method Using Charge Restraints for Deriving Atomic Charges: The RESP Model. *J. Phys. Chem.* **1993**, *97*, 10269–10280.
- (43) Berendsen, H. J. C.; van der Spoel, D.; van Drunen, R. GROMACS: A Message-Passing Parallel Molecular Dynamics Implementation. *Comput. Phys. Commun.* **1995**, *91*, 43–56.
- (44) Hess, B.; Kutzner, C.; van der Spoel, D.; Lindahl, E. GROMACS 4: Algorithms for Highly Efficient, Load-Balanced, and Scalable Molecular Simulation. *J. Chem. Theory Comput.* **2008**, 4, 435–447.
- (45) Pronk, S.; Páll, S.; Schulz, R.; Larsson, P.; Bjelkmar, P.; Apostolov, R.; Shirts, M. R.; Smith, J. C.; Kasson, P. M.; van der Spoel, D.; Hess, B.; Lindahl, E. GROMACS 4.5: A High-Throughput

- and Highly Parallel Open Source Molecular Simulation Toolkit. *J. Bioinf.* **2013**, *29*, 845–854.
- (46) Hess, B.; Bekker, H.; Berendsen, H. J. C. LINCS: A Linear Constraint Solver for Molecular Simulations. *J. Comput. Chem.* **1997**, 14, 1463.
- (47) Darden, T.; York, D.; Pedersen, L. Particle Mesh Ewald: An Nlog(N) Method for Ewald Sums in Large Systems. *J. Chem. Phys.* **1993**, *98*, 10089–10092.
- (48) Evans, D.; Holian, B. The Nose-Hoover Thermostat. *J. Chem. Phys.* **1985**, 83, 4069–4074.
- (49) Parrinello, M.; Rahman, A. Crystal Structure and Pair Potentials: A Molecular-Dynamics Study. *Phys. Rev. Lett.* **1980**, 45, 1196–1199.
- (50) Cheatham, T. E.; Cieplak, P.; Kollman, P. A. A Modified Version of the Cornell et al. Force Field with Improved Sugar Pucker Phases and Helical Repeat. *J. Biomol. Struct. Dyn.* **1999**, *16*, 845–862.
- (51) Bas, D. C.; Rogers, D. M.; Jensen, J. H. Very Fast Prediction and Rationalization of PKa Values for Protein-Ligand Complexes. *Proteins* **2008**, *73*, 765-783.
- (52) Svishchev, I. M.; Kusalik, P. G. Structure in Liquid Water: A Study of Spatial Distribution Functions. *J. Chem. Phys.* **1993**, *99*, 3049–3058.
- (53) Robinson, J. R.; Karkov, H. S.; Woo, J. A.; Krogh, B. O.; Cramer, S. M. QSAR Models for Prediction of Chromatographic Behavior of Homologous Fab Variants. *Biotechnol. Bioeng.* **2017**, *114*, 1231–1240
- (54) Patel, A. J.; Garde, S. Efficient Method to Characterize the Context-Dependent Hydrophobicity of Proteins. *J. Phys. Chem. B* **2014**, *118*, 1564–1573.
- (55) Potterton, A.; Husseini, F. S.; Southey, M. W. Y.; Bodkin, M. J.; Heifetz, A.; Coveney, P. V.; Townsend-Nicholson, A. Ensemble-Based Steered Molecular Dynamics Predicts Relative Residence Time of A Receptor Binders. *J. Chem. Theory Comput.* **2019**, *15*, 3316–3330.
- (56) Monroe, J. I.; Shell, M. S. Computational Discovery of Chemically Patterned Surfaces That Effect Unique Hydration Water Dynamics. *Proc. Natl. Acad. Sci. U.S.A.* **2018**, *115*, 8093–8098.
- (57) Bortolato, A.; Deflorian, F.; Weiss, D. R.; Mason, J. S. Decoding the Role of Water Dynamics in Ligand-Protein Unbinding: CRF <sub>1</sub> R as a Test Case. *J. Chem. Inf. Model.* **2015**, *55*, 1857–1866.
- (58) Russo, D.; Murarka, R. K.; Copley, J. R. D.; Head-Gordon, T. Molecular View of Water Dynamics near Model Peptides. *J. Phys. Chem. B* **2005**, *109*, 12966–12975.
- (59) Parimal, S.; Garde, S.; Cramer, S. M. Interactions of Multimodal Ligands with Proteins: Insights into Selectivity Using Molecular Dynamics Simulations. *Langmuir* **2015**, *31*, 7512–7523.
- (60) Gudhka, R. B.; Roush, D. J.; Cramer, S. M. A Thermodynamic Evaluation of Antibody-Surface Interactions in Multimodal Cation Exchange Chromatography. *J. Chromatogr. A* **2020**, *1628*, 461479.
- (61) Bilodeau, C. L.; Lau, E. Y.; Roush, D.; Garde, S.; Cramer, S. M. Formation of Ligand Clusters on Multimodal Chromatographic Surfaces. *Langmuir* **2019**, *35*, 16770–16779.

## ■ NOTE ADDED AFTER ASAP PUBLICATION

Published ASAP on June 7, 2021; Revised June 17, 2021 to correct equation in Results and Discussion.